LETTER

High–throughput decoding of antitrypanosomal drug efficacy and resistance

Sam Alsford[1], Sabine Eckert[2]†, Nicola Baker[1], Lucy Glover[1], Alejandro Sanchez-Flores[2], Ka Fai Leung[3], Daniel J. Turner[2]†, Mark C. Field[3], Matthew Berriman[2] & David Horn[1]

The concept of disease-specific chemotherapy was developed a century ago. Dyes and arsenical compounds that displayed selectivity against trypanosomes were central to this work[1,2], and the drugs that emerged remain in use for treating human African trypanosomiasis (HAT)[3]. The importance of understanding the mechanisms underlying selective drug action and resistance for the development of improved HAT therapies has been recognized, but these mechanisms have remained largely unknown. Here we use all five current HAT drugs for genome-scale RNA interference target sequencing (RIT-seq) screens in *Trypanosoma brucei*, revealing the transporters, organelles, enzymes and metabolic pathways that function to facilitate antitrypanosomal drug action. RIT-seq profiling identifies both known drug importers[4,5] and the only known pro-drug activator[6], and links more than fifty additional genes to drug action. A bloodstream stage-specific invariant surface glycoprotein (ISG75) family mediates suramin uptake, and the AP1 adaptin complex, lysosomal proteases and major lysosomal transmembrane protein, as well as spermidine and *N*-acetylglucosamine biosynthesis, all contribute to suramin action. Further screens link ubiquinone availability to nitro-drug action, plasma membrane P-type H^+-ATPases to pentamidine action, and trypanothione and several putative kinases to melarsoprol action. We also demonstrate a major role for aquaglyceroporins in pentamidine and melarsoprol cross-resistance. These advances in our understanding of mechanisms of antitrypanosomal drug efficacy and resistance will aid the rational design of new therapies and help to combat drug resistance, and provide unprecedented molecular insight into the mode of action of antitrypanosomal drugs.

African trypanosomes are transmitted by the tsetse insect vector and circulate in the bloodstream and tissue fluids of their mammalian hosts. These protozoan parasites cause HAT, also known as sleeping sickness, and the livestock disease known as Nagana. HAT is typically fatal if there is no chemotherapeutic intervention. The public health situation has improved recently with increased monitoring and chemotherapy averting more than 1.3 million disability-adjusted life years (DALYs) in the year 2000 and the estimated number of cases at less than 70,000 in 2006 (ref. 7). However, therapies have many problems, including severe toxicity and increasing resistance, which is a major concern owing to the absence of a vaccine or therapeutic alternatives[3]. The current HAT therapies are pentamidine or suramin, which are only suitable for the first stage of the disease before central nervous system involvement, and eflornithine, nifurtimox or melarsoprol for advanced disease[3] (Supplementary Table 1). All of these drugs were developed well before the advent of molecular, target-based therapy and, with the exception of eflornithine, they elicit their antitrypanosomal effects by disrupting unknown targets. HAT treatment failure rates were reported to be increasing for suramin, when this drug was still in use in West Africa in the 1950s[8], and melarsoprol treatment failure is a current and increasing problem[9].

We used genome-scale tetracycline-inducible RNA interference (RNAi) library screens in *T. brucei* to identify the genes that contribute to drug action. In these screens, replicating cells only persist in an otherwise toxic environment if knockdown confers a selective advantage (Fig. 1a); note that knockdown is not expected to identify drug targets. The RNAi library consists of ~750,000 clones, each transformed with one RNAi construct, and represents >99% of the approximately 7,500 non-redundant *T. brucei* gene set. Because each gene is identified by an average of approximately five different RNAi sequences, true leads can be identified with high confidence and potential off-target false leads can be minimized (see Supplementary Methods). Screens were performed using all current HAT drugs and each yielded a population of cells displaying an inducible drug resistance phenotype after eight or fourteen days of selection (Fig. 1b and Supplementary Fig. 1). Genomic DNA from these cells was subjected to RIT-seq[10] to create profiles of RNAi targets associated with increased resistance and to identify the genes that contribute to drug susceptibility. Genome-wide association maps show read density for 7,435 *T. brucei* genes (Fig. 1c). We defined genes with 'primary signatures' as those associated with two or more independent RIT-seq tags, each with a read density of >99; the screens yielded 55 of these signatures (Fig. 1c; see Supplementary Methods and Supplementary Data 1. Previous work linked the P2 adenosine transporter 1 (AT1) to melarsoprol uptake[4,11–13], an amino acid transporter family member (AAT6) to eflornithine uptake[5,13,14] and a nitroreductase (NTR) to nifurtimox activation[6,14]. Each of these genes is identified on the appropriate genome-wide association map (Fig. 1c), providing validation for our screens and indicating excellent genome-scale coverage in the RNAi library. Selected read-density signatures that establish new genetic links to drug susceptibility are shown in Fig. 1d.

The known eflornithine transporter is the only primary signature from the eflornithine screen. By contrast, the suramin screen revealed 28 genes associated with primary signatures (Fig. 1c and Supplementary Data 1). Suramin, which has been used for HAT therapy since the 1920s[15], is a colourless sulphated napthylamine related to trypan red. Because this drug has a strong negative charge, it cannot cross lipid membranes by passive diffusion. Genes that are linked to the action of suramin encode ISG75, the function of which is unknown[16], four lysosomal proteins (the cathepsin L (CatL) and CBP1 peptidases, p67 and Golgi/lysosomal protein 1 (GLP1)), all four subunits of the adaptin complex (AP1), which are involved in endosomal, clathrin-mediated trafficking, and multiple spermidine and *N*-acetylglucosamine biosynthetic enzymes (Supplementary Fig. 2 and Supplementary Data 1).

Eight of these genes were selected for further analysis. We assembled multiple independent inducible RNAi strains for each gene and confirmed that knockdown (Fig. 2a and Supplementary Fig. 3) increased suramin resistance in every case (Fig. 2b and Supplementary Fig. 4). We then determined subcellular localization for the putative major facilitator superfamily transporter (MFST); the tandem of three closely
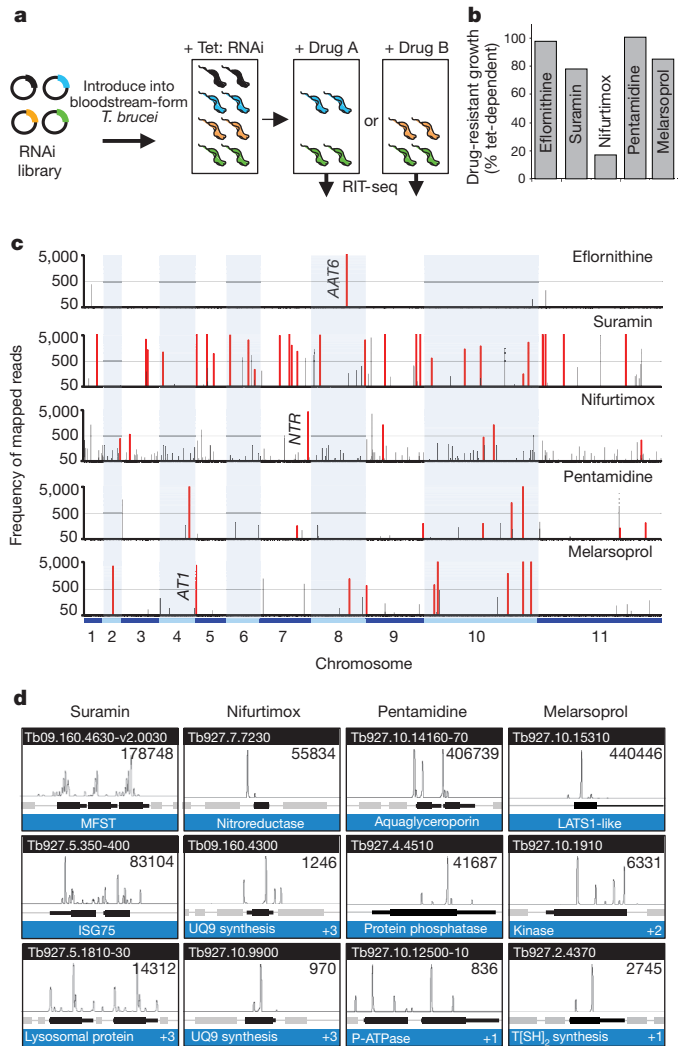
Figure 1 | Identification of drug efficacy determinants in *T. brucei*. a, A schematic showing the RNAi library screening approach. The expected outcomes are given for RNAi targets that fail to affect drug resistance (black), increase resistance to drug A (blue), drug B (orange) or both (green). **b**, Each screen yielded a population displaying tetracycline (Tet)-inducible (RNAi-dependent) drug-resistance (see Supplementary Fig. 1). The plot indicates the proportion of the resistance phenotype that is tetracycline inducible. **c**, Genome-wide RIT-seq profiles. Each map represents a non-redundant set of 7,435 protein-coding sequences. Red bars represent 'primary' read-density signatures. Black bars represent all other signatures of >50 reads (see Supplementary Data 1). All three expected 'hits', *AAT6*, *AT1* and *NTR*, are indicated. **d**, Selected signatures. Each peak represents a unique RIT-seq tag. '+', numbers of additional genes identified in each category. See Supplementary Fig. 2 for details and additional signatures.

related *MFST* genes gave the strongest read-density signature in the suramin screen and the greatest half-maximum effective concentration (EC_{50}) increase (> tenfold) following knockdown (Fig. 2b). In contrast to a putative ubiquitin hydrolase (UBH1) identified by the screen, MFST and a member of the endomembrane EMP70 family partitioned into the *T. brucei* membrane fraction, as expected (Fig. 2c), and MFST localized to the lysosome as did the major lysosomal type I membrane glycoprotein, p67 (ref. 17), which was also identified in the screen (Fig. 2d). Because ISG75 trafficking is ubiquitin dependent[18], we investigated whether UBH1 influenced ISG75 expression. UBH1 knockdown reduced ISG75 but not ISG65 expression (Fig. 2e), suggesting that de-ubiquitination by UBH1 specifically affects ISG75 copy number; clearly this mimics the direct effect of RNAi against ISG75. A vacuolar protein sorting factor, Vps5, which positively controls ISG75 expression[19], and a second putative ubiquitin hydrolase, were
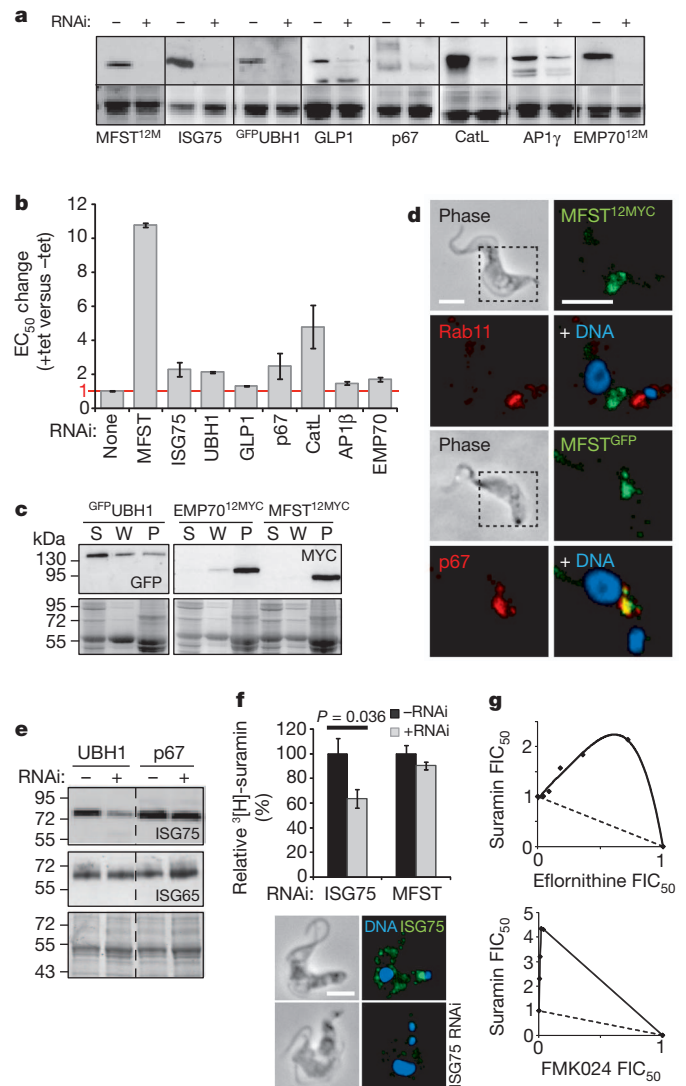

Figure 2 | A network of proteins link ISG75, endocytosis and lysosomal functions to suramin action. a, Western blots demonstrate knockdown; Coomassie stains serve as loading controls. Tags, green fluorescent protein (GFP) and 12×MYC epitope (12M). See Supplementary Fig. 3 for growth curves. **b**, Endosomal and lysosomal factors and ISG75 contribute to suramin action. Error bars, s.d. from independent RNAi strains (see Supplementary Fig. 4). **c**, MFST and EMP70 are membrane associated. The western blots show supernatant (S), wash (W) and pellet (P; membrane fraction). **d**, MFST co-localizes with lysosomal protein, p67, but not recycling endosomes (Rab11). Dashed boxes, areas magnified in fluorescent images. **e**, Knockdown of UBH1 specifically decreases ISG75 expression. **f**, ISG75 mediates suramin binding. Error bars, s.d. from duplicate experiments. *P* value from Student's *t*-test. ISG75 knockdown is shown. Scale bar, 5 μm. **g**, The CatL–CatB, and ODC inhibitors FMK024 and eflornithine, respectively, antagonize suramin action. Isobolograms showing 50% fractional inhibitory concentrations (FICs). The solid lines indicate antagonism. The dashed lines indicate expected outcomes for no interaction.

also identified by the screen (see Supplementary Fig. 2 and Supplementary Data 1), suggesting that ISG75 copy number is highly connected to suramin resistance. To investigate whether ISG75 contributes to suramin binding, we performed whole-cell binding assays using ³[H]-labelled suramin. Cells that were depleted for ISG75 displayed significantly and specifically reduced suramin binding (Fig. 2f).

We observed a greater than fourfold increase in EC_{50} after knockdown of the CatL-like protease known as brucipain, another abundant lysosomal protein[20], and an orthogonal assay using a dual-specificity CatL–CatB inhibitor revealed inhibitor antagonism (Fig. 2g), indicating that protease activity enhances suramin toxicity. Taken together, the

results demonstrate a central role for lysosomal functions in suramin action. As four enzymes that are involved in spermidine biosynthesis, including ornithine decarboxylase (ODC), were linked to suramin action (Supplementary Data 1), we used eflornithine to specifically inhibit ODC, which again revealed inhibitor antagonism (Fig. 2g; Supplementary Table 1). Thus, ODC activity enhances suramin toxicity, probably through spermidine biosynthesis. Suramin endocytosis[21] and intralysosomal accumulation[22] have previously been demonstrated in *T. brucei* and an acquired suramin resistance phenotype was stable in bloodstream stage *T. brucei* but was not expressed in the insect stage[23]. The RIT-seq profile reported here, bloodstream-stage-specific expression of ISG75[16] and strong downregulation of endocytic and lysosomal activities in the insect stage[24], are all consistent with stage-specific, intralysosomal accumulation of suramin.

Work with dyes and arsenicals revealed the first examples of resistance to chemotherapy a century ago and, based on cross-resistance, it was deduced that there are shared mechanisms contributing to the action of certain 'parasitotropic' compounds[1]. Among current HAT therapies, cross-resistance has been documented only for melarsoprol and pentamidine[9], but our understanding of the mechanism remains incomplete. Both drugs enter trypanosomes through the P2 AT1 but additional, dual-specificity transporters are predicted[9]. To identify cross-resistance mechanisms, we analysed all pair-wise comparisons among our screens (Fig. 3a). A single robust signature emerged, implicating two closely related aquaglyceroporins (AQPs)[25] in melarsoprol and pentamidine cross-resistance. To directly test the role of the AQPs, we generated a strain that was deficient in *aqp2* and *aqp3* (*aqp2/aqp3*-null strain) (Fig. 3b). The EC$_{50}$ was increased more than 2-fold and 15-fold for melarsoprol and pentamidine, respectively, in *aqp2/aqp3*-null cells compared to wild-type cells (Fig. 3c). Our favoured hypothesis involves regulation of dual-specificity transporters by AQPs.

The nifurtimox, pentamidine and melarsoprol screens yielded eight, nine and nine genes associated with primary signatures, respectively. The major primary signature in the nifurtimox profile identified the mitochondrial, flavin-dependent nitroreductase that activates this class of nitro pro-drugs[6]. We also identified the putative flavokinase that converts riboflavin to FMN, an essential nitroreductase cofactor[6]. Four additional signatures identified genes that encode proteins linked to ubiquinone biosynthesis (Supplementary Fig. 2 and Supplementary Data 1), in support of the hypothesis that nitroreductase, like NADH dehydrogenases, transfers electrons from NADH to ubiquinone to generate ubiquinol[6]. We assembled RNAi strains for one of these factors and demonstrated that knockdown increased the EC$_{50}$ for nifurtimox by approximately 1.5-fold (Supplementary Fig. 5). Thus, six gene signatures support a dominant role for nitroreductase in nifurtimox activation and suggest that this is dependent upon the availability of the FMN cofactor and the natural substrate.

Pentamidine is an aromatic diamidine, a nucleic acid binding drug that accumulates to millimolar concentrations and collapses trypanosome mitochondrial membrane potential[26]. Two primary signatures from the pentamidine screen identify genes encoding P-type ATPases (Supplementary Fig. 2 and Supplementary Data 1), and one of these represents the plasma membrane H$^+$-ATPases, HA1, HA2 and HA3 (ref. 27). We assembled RNAi strains for these ATPases and demonstrated that knockdown increased the EC$_{50}$ for pentamidine more than eightfold (Supplementary Fig. 5), suggesting that an HA1–3 dependent proton motive force is required to drive pentamidine uptake. We used a similar approach to demonstrate a greater than twofold increase in the EC$_{50}$ for pentamidine following knockdown of a putative protein phosphatase (Supplementary Fig. 5).

Melarsoprol acts primarily by forming a stable adduct with trypanothione, known as Mel T[28], but whether this adduct reduces or increases toxicity has remained unclear. The melarsoprol screen identified a link to trypanothione synthase and trypanothione reductase (Supplementary Fig. 2 and Supplementary Data 1), suggesting that the Mel T adduct is toxic. Three other primary signatures identified an
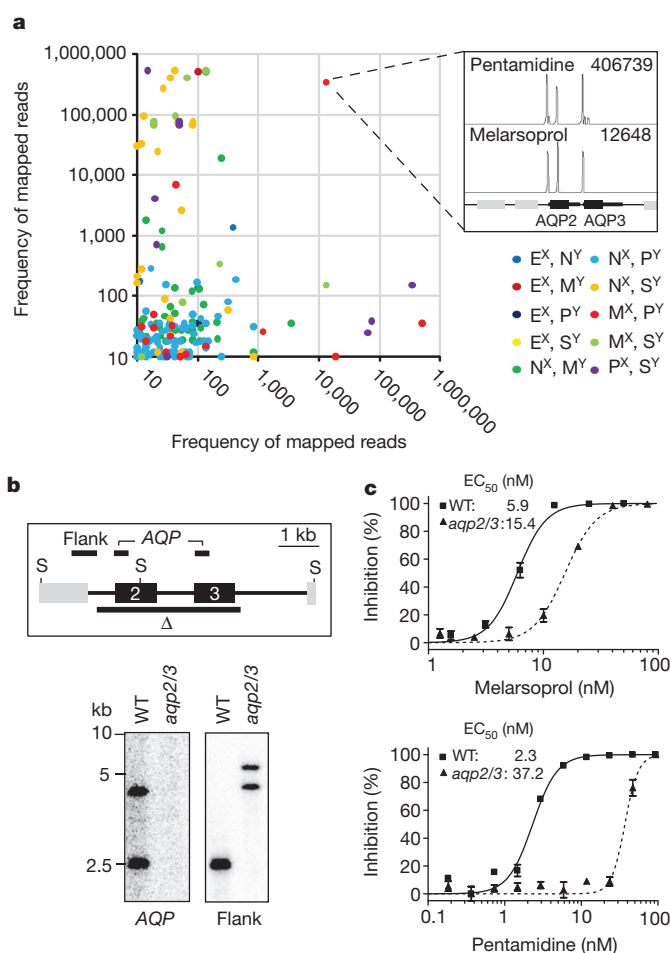

Figure 3 | *aqp2/aqp3*-null cells are melarsoprol, pentamidine cross-resistant. a, Analysis of read density for all (74,350) possible pair-wise comparisons of a non-redundant *T. brucei* gene set. E, eflornithine; M, melarsoprol; N, nifurtimox; P, pentamidine; S, suramin; ^{X} and ^{Y}, axes representing each data set. The box on the right shows the read-density signatures for this locus (Tb927.10.14160-70). **b**, AQP2 and AQP3 knockout was confirmed by Southern blot analysis. Δ, the region deleted; S, *SacII*; WT, wild type. Bars indicate probes. **c**, EC$_{50}$ analysis indicates melarsoprol, pentamidine cross-resistance in *aqp2/aqp3*-null cells. Error bars, s.d. from triplicate assays and independent null strains.

over-representation ($P = 2.3 \times 10^{-9}$, χ^2 test) of putative protein kinases (Supplementary Fig. 2 and Supplementary Data 1), and another signature identified a gene encoding a highly phosphorylated protein related to the amino-terminal segment of the large tumour suppressor, LATS1 (see Supplementary Fig. 2a). We used independent strains to confirm that LATS1-like knockdown increased the EC$_{50}$ for melarsoprol by approximately 1.5-fold (Supplementary Fig. 5). On the basis of these signatures, we suggest a role for a signalling cascade in melarsoprol susceptibility. Our findings are summarized in Fig. 4. In particular, we propose that suramin uptake occurs through ISG75-mediated endocytosis (Fig. 4a). Metabolic pathways that contribute to suramin or nifurtimox action are detailed in Fig. 4b.

All but one of the current HAT drugs was developed in the absence of an understanding of the chemical–biological relationships underlying toxicity or selectivity. Our RIT-seq profiles revealed more than 50 *T. brucei* genes that enhance drug susceptibility, unearthing interactions that are largely inaccessible using other approaches. Notably, the knockdown approach and the sensitivity of RIT-seq allow access to essential proteins, complexes and pathways such as H$^+$-ATPase, the adaptin complex and spermidine biosynthesis. Our results also show the utility of drugs as molecular probes for functional networks. In particular, the findings highlight factors that contribute to drug
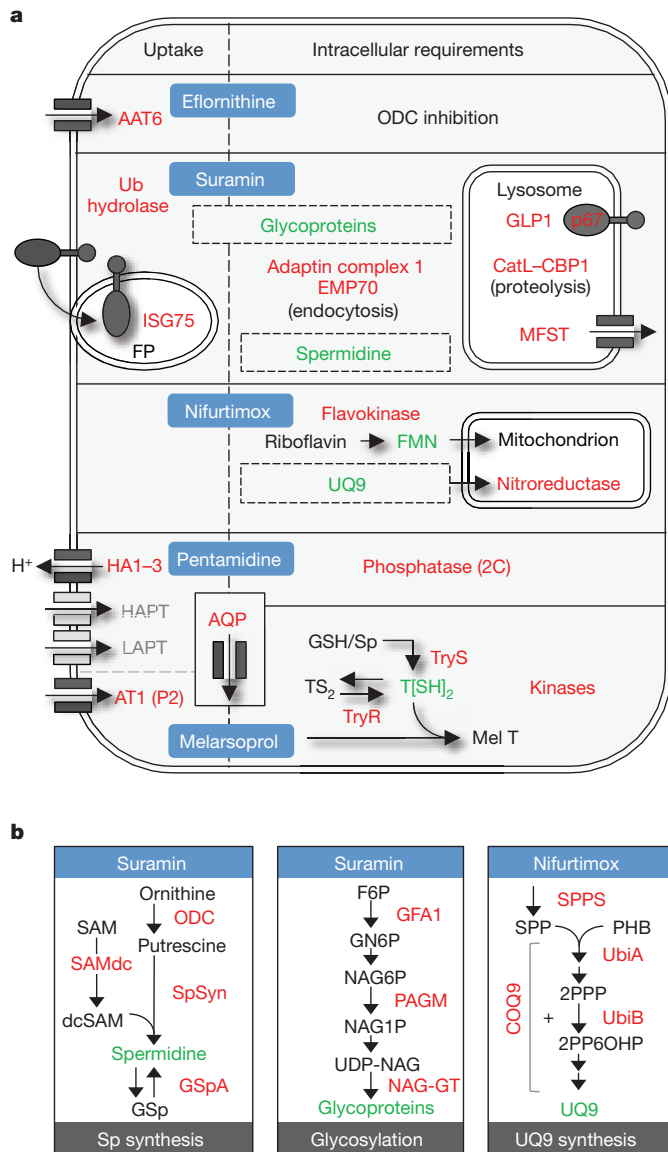
Figure 4 | Determinants of drug efficacy in African trypanosomes.
a, b, Proteins (red) and metabolites (green) that are linked to drug action. **a**, A schematic summarizing the findings from the RIT-seq screens. In the case of suramin, we propose that ISG75 binds the drug at the cell surface. ISG75 trafficking then delivers the complex, through the flagellar pocket (FP), to the endosomal system, leading to accumulation in the lysosome where the drug is liberated by proteases. The MFST may deliver the drug to the cytosol. HAPT, high-affinity pentamidine transporter; LAPT, low-affinity pentamidine transporter; TS_2, oxidised trypanothione; $T[SH]_2$, reduced trypanothione; UQ9, ubiquinone 9. **b**, Biosynthetic pathways that are linked to drug action. See Supplementary Data 1 for definitions and further details.

accumulation or the generation of toxic metabolites, features that could be exploited to deliver or generate novel toxins. Additionally, absence or loss of function could explain innate or acquired resistance; suramin resistance or melarsoprol and pentamidine cross-resistance may be due to reduced MFST or AQP expression, respectively (for examples, see Supplementary Fig. 6). These advances in our understanding of drug–trypanosome interactions will facilitate rational approaches to the design of more efficacious and durable therapies, and will be useful for monitoring the emergence and spread of resistance.

METHODS SUMMARY

Assembly of the bloodstream-form *T. brucei* RNAi library and RIT-seq were reported previously[10]. Briefly, a tetracycline-inducible RNAi plasmid library,

containing randomly sheared genomic fragments (with a mean fragment size of ~600 bp) under the control of head-to-head, tetracycline-inducible phage T7 promoters[29], was targeted to a single genomic locus that had been validated for robust expression[30]. The long double-stranded RNAs (dsRNAs) that were generated in the presence of tetracycline are processed to produce a pool of short interfering RNAs that programme the endogenous RNAi machinery to mediate sequence-specific destruction of the cognate messenger RNA. For this study, the library was grown under inducing conditions with drug selection, and genomic DNA was isolated from surviving populations. For RIT-seq profiling, adaptor-ligated sequencing libraries were prepared from each genomic DNA sample and used to amplify DNA fragments containing RNAi cassette-insert junctions in semi-specific PCR reactions; one primer was specific for the RNAi vector and the other for the Illumina adaptor. Size-selected DNA was sequenced with 76 cycle runs on an Illumina GAII. Sequencing reads containing a nine-base RNAi cassette-insert junction sequence were then mapped to the *T. brucei* reference genome. In cases in which loss of function increases drug tolerance, RNAi-target sequence representation is increased relative to the otherwise susceptible population, revealing 'hot spots'. Thus, RNAi target fragments serve as templates for the production of dsRNA and also provide unique sequence identifiers for each clonal population.

Full Methods and any associated references are available in the online version of the paper at www.nature.com/nature.

1. Ehrlich, P. Address in pathology, on chemiotherapy: delivered before the seventeenth international congress of medicine. *BMJ* **2**, 353–359 (1913).
2. Williamson, J. in *The African Trypanosomiases* (ed. Mulligan, H. W.) (Allen and Unwin, 1970).
3. Fairlamb, A. H. Chemotherapy of human African trypanosomiasis: current and future prospects. *Trends Parasitol.* **19**, 488–494 (2003).
4. Mäser, P., Sutterlin, C., Kralli, A. & Kaminsky, R. A nucleoside transporter from *Trypanosoma brucei* involved in drug resistance. *Science* **285**, 242–244 (1999).
5. Vincent, I. M. *et al.* A molecular mechanism for eflornithine resistance in African trypanosomes. *PLoS Pathog.* **6**, e1001204 (2010).
6. Wilkinson, S. R., Taylor, M. C., Horn, D., Kelly, J. M. & Cheeseman, I. A mechanism for cross-resistance to nifurtimox and benznidazole in trypanosomes. *Proc. Natl Acad. Sci. USA* **105**, 5022–5027 (2008).
7. Fèvre, E. M., Wissmann, B. V., Welburn, S. C. & Lutumba, P. The burden of human African trypanosomiasis. *PLoS Negl. Trop. Dis.* **2**, e333 (2008).
8. Pépin, J. & Milord, F. The treatment of human African trypanosomiasis. *Adv. Parasitol.* **33**, 1–47 (1994).
9. de Koning, H. P. Ever-increasing complexities of diamidine and arsenical crossresistance in African trypanosomes. *Trends Parasitol.* **24**, 345–349 (2008).
10. Alsford, S. *et al.* High-throughput phenotyping using parallel sequencing of RNA interference targets in the African trypanosome. *Genome Res.* **21**, 915–924 (2011).
11. Carter, N. S. & Fairlamb, A. H. Arsenical-resistant trypanosomes lack an unusual adenosine transporter. *Nature* **361**, 173–176 (1993).
12. Matovu, E. *et al.* Mechanisms of arsenical and diamidine uptake and resistance in *Trypanosoma brucei*. *Eukaryot. Cell* **2**, 1003–1008 (2003).
13. Schumann Burkard, G., Jutzi, P. & Roditi, I. Genome-wide RNAi screens in bloodstream form trypanosomes identify drug transporters. *Mol. Biochem. Parasitol.* **175**, 91–94 (2011).
14. Baker, N., Alsford, S. & Horn, D. Genome-wide RNAi screens in African trypanosomes identify the nifurtimox activator NTR and the eflornithine transporter AAT6. *Mol. Biochem. Parasitol.* **176**, 55–57 (2011).
15. Steverding, D. The development of drugs for treatment of sleeping sickness: a historical review. *Parasit. Vectors* **3**, 15 (2010).
16. Overath, P., Chaudhri, M., Steverding, D. & Ziegelbauer, K. Invariant surface proteins in bloodstream forms of *Trypanosoma brucei*. *Parasitol. Today* **10**, 53–58 (1994).
17. Peck, R. F. *et al.* The LAMP-like protein p67 plays an essential role in the lysosome of African trypanosomes. *Mol. Microbiol.* **68**, 933–946 (2008).
18. Leung, K. F., Riley, F. S., Carrington, M. & Field, M. C. Ubiquitylation and developmental regulation of invariant surface protein expression in trypanosomes. *Eukaryot. Cell* **10**, 916–931 (2011).
19. Koumandou, V. L. *et al.* Evolutionary reconstruction of the retromer complex and its function in *Trypanosoma brucei*. *J. Cell Sci.* **124**, 1496–1509 (2011).
20. Caffrey, C. R. *et al.* Active site mapping, biochemical properties and subcellular localization of rhodesain, the major cysteine protease of *Trypanosoma brucei rhodesiense*. *Mol. Biochem. Parasitol.* **118**, 61–73 (2001).
21. Fairlamb, A. H. & Bowman, I. B. Uptake of the trypanocidal drug suramin by bloodstream forms of *Trypanosoma brucei* and its effect on respiration and growth rate *in vivo*. *Mol. Biochem. Parasitol.* **1**, 315–333 (1980).
22. Vansterkenburg, E. L. *et al.* The uptake of the trypanocidal drug suramin in combination with low-density lipoproteins by *Trypanosoma brucei* and its possible mode of action. *Acta Trop.* **54**, 237–250 (1993).

23. Scott, A. G., Tait, A. & Turner, C. M. Characterisation of cloned lines of *Trypanosoma brucei* expressing stable resistance to MelCy and suramin. *Acta Trop.* **60,** 251–262 (1996).
24. Natesan, S. K., Peacock, L., Matthews, K., Gibson, W. & Field, M. C. Activation of endocytosis as an adaptation to the mammalian host by trypanosomes. *Eukaryot. Cell* **6,** 2029–2037 (2007).
25. Uzcategui, N. L. *et al.* Cloning, heterologous expression, and characterization of three aquaglyceroporins from *Trypanosoma brucei. J. Biol. Chem.* **279,** 42669–42676 (2004).
26. Lanteri, C. A., Tidwell, R. R. & Meshnick, S. R. The mitochondrion is a site of trypanocidal action of the aromatic diamidine DB75 in bloodstream forms of *Trypanosoma brucei. Antimicrob. Agents Chemother.* **52,** 875–882 (2008).
27. Luo, S., Fang, J. & Docampo, R. Molecular characterization of *Trypanosoma brucei* P-type H^+-ATPases. *J. Biol. Chem.* **281,** 21963–21973 (2006).
28. Fairlamb, A. H., Henderson, G. B. & Cerami, A. Trypanothione is the primary target for arsenical drugs against African trypanosomes. *Proc. Natl Acad. Sci. USA* **86,** 2607–2611 (1989).
29. Morris, J. C., Wang, Z., Drew, M. E. & Englund, P. T. Glycolysis modulates trypanosome glycoprotein expression as revealed by an RNAi library. *EMBO J.* **21,** 4429–4438 (2002).
30. Alsford, S., Kawahara, T., Glover, L. & Horn, D. Tagging a *T. brucei RRNA* locus improves stable transfection efficiency and circumvents inducible expression position effects. *Mol. Biochem. Parasitol.* **144,** 142–148 (2005).

METHODS

***T. brucei* growth and drug selection.** The bloodstream-form *T. brucei* MITat 1.2 clone 221a RNAi library[10] was derived using the randomly sheared genomic fragment (with mean fragment length ~600 bp) RNAi plasmid library[29]. The *T. brucei* RNAi library and 2T1 cells were maintained as described[29,30]. For selective screens, the RNAi library, maintained throughout at $>5 \times 10^6$ cells, was induced with tetracycline (1 µg ml^{-1}) for 24 h and then grown in medium containing tetracycline, plus each HAT drug at $0.5 \times EC_{50}$ to $3.5 \times EC_{50}$ (Supplementary Table 1 and Supplementary Fig. 1). All drug stocks were in dimethylsulphoxide.

RIT-seq. Selected populations from each screen were assessed for tetracycline-dependent drug resistance. The RNAi target fragments provide unique identifiers for each clone in the population. As a quality-control step, PCR amplification, agarose gel fractionation and Sanger sequencing of the eluted products were performed as described[14], and followed with RIT-seq analysis[10]. All nine genes that were identified by Sanger sequencing were associated with high-density Illumina read-counts (13,000 to 528,000; see Supplementary Data 1a). Briefly, we ran 76-cycle sequencing on an Illumina GAII; this generates sequence tags derived from the ends of the RNAi target fragments. Only sequences containing a terminal RNAi-vector junction sequence (GCCTCGCGA) were mapped to the *T. brucei* 927 reference genome[31] using the SSAHA sequence alignment algorithm[32]. After mapping, for each protein coding sequence (CDS) in each experiment, we obtained a count of reads mapping; all genes associated with >9 reads are detailed in Supplementary Data 1b. We also browsed all read-density plots in Artemis[33] for signatures that fell outside of CDSs to generate the full non-redundant 'hit list' detailed in Supplementary Data 1a.

Read-density signatures. Genome coverage in the current RNAi library represents >99% of all genes, with 5 RNAi targets per gene on average[10]; shorter genes are expected to be represented by fewer RNAi targets. Our screens yielded 5–59 genes (0.07–0.8%) with a $^{>99}$RIT-seq tag (a tag with a read density of >99; the eflornithine screen yielded 5, the suramin screen 59 the nifurtimox screen 54, the pentamidine screen 17 and the melarsoprol screen 19). In each screen, at least one gene was associated with a $^{>50,000}$RIT-seq tag (Supplementary Data 1a). From this set, we derived 55 genes with 'primary signatures', those associated with two or more $^{>99}$RIT-seq tags. If these tags were randomly distributed, we would expect a single primary signature from 300 screens using eflornithine or from two screens using suramin, assigning a high degree of confidence to the vast majority of observed primary signatures (Supplementary Data 1a). The nifurtimox output is unusual compared to the other outputs and may reflect drug-mediated mutagenesis[34]; for example, inactivating mutations within *NTR* may prolong the survival of clones carrying unrelated RNAi targets. However, even limited tetracycline-regulated drug resistance (Fig. 1b) and a high number of sequence tags in the nifurtimox screening profile (Supplementary Data 1 and Fig. 1c) had little impact on primary signature confidence. Many of the 130 genes that are associated with 'secondary signatures' in Supplementary Data 1a may also reflect mechanisms of drug action, but here we only considered seven of these genes that were linked to a common function with a primary hit (Supplementary Fig. 2). We observe that, on average, 3.5 tags per gene are associated with the 24 primary, single copy genes that are shown in Supplementary Fig. 2. Minimal library propagation could explain a modest reduction in coverage but we suggest that reduced coverage in the current RIT-seq outputs is primarily explained by major fitness defects following knockdown.

Plasmid construction and strain assembly. The *AQP* locus was disrupted by replacement of a 4,772-bp (*AQP2* and *AQP3*) fragment with *NPT* and *BLA* selectable markers (the *T. brucei* genome is diploid). Gene-specific RNAi fragments of 400–600 bp or 200 bp, to facilitate moderate knockdown in the case of the known essential gene p67 (ref. 17), were amplified using PCR primers designed using RNAit[35] and cloned into pRPaiSL for the generation of stem-loop, 'hairpin' dsRNA as the trigger for RNAi[36]. We used a long, 400–600-bp RNAi target fragment for CatL because RNAi previously produced no growth defect[37]. However, cells retained 35% CatL activity in that study[37], probably explaining why we see a major growth defect when expressing a more potent stem-loop dsRNA (Supplementary Fig. 3). For epitope tagging at native loci, C-terminal fragments, or an N-terminal fragment (UBH1), were amplified and cloned in pNATx^{TAG} and pNAT^{TAG}x (ref. 36), respectively. Constructs were introduced into 2T1 cells as described[30]. Full oligonucleotide details are available on request.

Strain analysis. Cumulative growth curves were generated from cultures seeded at 10^5 cells ml^{-1}, counted on a haemocytometer and diluted back to 10^5 cells ml^{-1} as necessary. For EC$_{50}$ assays, RNAi strains were pre-induced for 72 h in 1 µg ml^{-1} tetracycline, except CatL and AP1β, which were pre-induced for 24 h at 2.5 and 1 ng ml^{-1}, respectively. Isobolograms were generated using a checkerboard assay as described[38]; FMK024 (*N*-morpholineurea-phenylalanyl-homophenylalanylfluoromethyl ketone; Sigma) is an irreversible, dual-specificity inhibitor of CatL and CatB. All EC$_{50}$ assays were carried out using alamarBlue as described[14,39]. Southern blotting was carried out according to standard procedures[40]. Subcellular fractionation by hypotonic lysis was carried out as described[41]. All protein samples were stored in the presence of a protease inhibitor cocktail (Roche) and were not boiled. Whole-cell lysates and hypotonic lysis fractions were separated by SDS–PAGE using standard protocols[40]. Immunofluorescence was carried out as previously described[10]. We used specific antisera to detect ISG75 (ref. 42), p67 (ref. 43), CatL[17], GLP1 (ref. 44) and AP1γ (ref. 45), and anti-MYC or anti-GFP antisera were used to detect tagged versions of MFST, UBH1 and EMP70. To assess suramin binding, cells were collected at mid-log phase and resuspended at 10^7 ml^{-1} in 35 nM ^{3}[H]-suramin (Hartmann Analytic; pre-incubated for 16 h in complete HMI11) at 37 °C. Cells were washed in ice-cold PBS, resuspended in 100 µl Optiphase Supermix scintillant (Perkin Elmer) and ^{3}[H]-suramin incorporation quantified using a 1450 Microbeta scintillation counter (Perkin Elmer).

31. Berriman, M. *et al.* The genome of the African trypanosome *Trypanosoma brucei*. *Science* **309,** 416–422 (2005).
32. Ning, Z., Cox, A. J. & Mullikin, J. C. SSAHA: a fast search method for large DNA databases. *Genome Res.* **11,** 1725–1729 (2001).
33. Carver, T. *et al.* Artemis and ACT: viewing, annotating and comparing sequences stored in a relational database. *Bioinformatics* **24,** 2672–2676 (2008).
34. Buschini, A. *et al.* Genotoxicity revaluation of three commercial nitroheterocyclic drugs: nifurtimox, benznidazole, and metronidazole. *J. Parasitol. Res.* **2009,** 463575 (2009).
35. Redmond, S., Vadivelu, J. & Field, M. C. RNAit: an automated web-based tool for the selection of RNAi targets in *Trypanosoma brucei*. *Mol. Biochem. Parasitol.* **128,** 115–118 (2003).
36. Alsford, S. & Horn, D. Single-locus targeting constructs for reliable regulated RNAi and transgene expression in *Trypanosoma brucei*. *Mol. Biochem. Parasitol.* **161,** 76–79 (2008).
37. Mackey, Z. B., O'Brien, T. C., Greenbaum, D. C., Blank, R. B. & McKerrow, J. H. A cathepsin B-like protease is required for host protein degradation in *Trypanosoma brucei*. *J. Biol. Chem.* **279,** 48426–48433 (2004).
38. Singh, P. K., Tack, B. F., McCray, P. B. Jr & Welsh, M. J. Synergistic and additive killing by antimicrobial factors found in human airway surface liquid. *Am. J. Physiol. Lung Cell. Mol. Physiol.* **279,** L799–L805 (2000).
39. Räz, B., Iten, M., Grether-Buhler, Y., Kaminsky, R. & Brun, R. The Alamar Blue assay to determine drug sensitivity of African trypanosomes (*T.b. rhodesiense* and *T.b. gambiense*) in vitro. *Acta Trop.* **68,** 139–147 (1997).
40. Ausubel, F. M., Brent, R., Kingston, R. E., Moore, D. D., Seidman, J. G., Smith, J. A. & Struhl, K. (eds) *Current Protocols in Molecular Biology* (John Wiley and Sons, 1998).
41. Leung, K. F., Dacks, J. B. & Field, M. C. Evolution of the multivesicular body ESCRT machinery; retention across the eukaryotic lineage. *Traffic* **9,** 1698–1716 (2008).
42. Ziegelbauer, K. & Overath, P. Organization of two invariant surface glycoproteins in the surface coat of *Trypanosoma brucei*. *Infect. Immun.* **61,** 4540–4545 (1993).
43. Kelley, R. J., Brickman, M. J. & Balber, A. E. Processing and transport of a lysosomal membrane glycoprotein is developmentally regulated in African trypanosomes. *Mol. Biochem. Parasitol.* **74,** 167–178 (1995).
44. Lingnau, A., Zufferey, R., Lingnau, M. & Russell, D. G. Characterization of tGLP-1, a Golgi and lysosome-associated, transmembrane glycoprotein of African trypanosomes. *J. Cell Sci.* **112,** 3061–3070 (1999).
45. Allen, C. L., Liao, D., Chung, W. L. & Field, M. C. Dileucine signal-dependent and AP-1-independent targeting of a lysosomal glycoprotein in *Trypanosoma brucei*. *Mol. Biochem. Parasitol.* **156,** 175–190 (2007).